Heavy Ion Beam Probe Diagnostic of Static and Dynamic Potential Structure

IGUCHI Harukazu*

National Institute for Fusion Science, 322-6 Oroshi-cho, Toki-shi 509-5292, Japan

Abstract

A heavy ion beam probe (HIBP) is a unique diagnostic method to measure the electric potential in magnetically confined high temperature plasmas. Its fine probing beam and well-collimated secondary beam detector give this diagnostic good spatial resolution, which together with the good time resolution make it powerful in probing plasma interior both in steady state and transient state. There are many excellent review papers [for example, 1,2], but these mostly concentrate on HIBP applications in tokamak research. The radial electric field or space potential structure is more important in stellarators or other non-axisymmetric tori, because particle fluxes are intrinsically non-ambipolar in these devices. This paper reports examples of HIBP measurements of potential structures in non-axisymmetric tori – the bumpy torus NBT-1M and the heliotron/torsatron CHS – following brief reviews of the development history and basic principles of the HIBP.

Keywords:

1. Introduction

The idea of using a heavy ion beam to probe the plasma interior originates from the work by R.L. Hickok and F.C. Jobes in 1960's. They injected a molecular hydrogen beam (H_2^+) at an energy of 2 MeV into a hollow cathode arc plasma, and detected protons produced by molecular break-up in the plasma, to measure plasma density and density fluctuations [3,4]. After that, they proposed to use a heavy ion beam with lower energy instead of a molecular hydrogen beam to measure plasma space potential and plasma density simultaneously [5]. The first application of the heavy ion beam probe (HIBP) to a magnetic confinement device was on the ST tokamak in early 1970's. Here, singly charged thallium ions (Tl^+) with an energy of 200 keV were used successfully to measure the space potential profile and density fluctuations associated with

an $m = 2$ tearing instability [6,7]. The systematic development of the HIBP diagnostic was continued by R.L. Hickok and his colleagues at Rensselaer Polytechnic Institute (RPI). In the late 1970's, they succeeded in measuring a two-dimensional space potential map in the ELMO Bumpy Torus (EBT) [8,9]. This attracted the attention and made this diagnostic popular, especially in the research of bumpy tori and tandem mirrors in the 1980's. HIBP's are now operational on the Nagoya Bumpy Torus (NBT) [10], the TMX tandem mirror [11], the RFC-XX tandem mirror with radio frequency plugging [12], the GAMMA-6 [13] and GAMMA-10 tandem mirrors [14]. In ISX-B the HIBP was applied to a tokamak plasma with neutral beam heating, where the consistency of the plasma potential profile measured with the HIBP with

*Corresponding author's e-mail: iguchi@nifs.ac.jp

the radial momentum balance equation and plasma toroidal/poloidal rotation velocity was demonstrated [15]. Recently, the radial momentum balance equation has been examined more precisely in the CHS heliotron/torsatron using a HIBP and charge exchange spectroscopy (CXS) [16]. Because of its high spatial and temporal resolution, and the capability to simultaneously measure the density and potential fluctuations together with their phase relations, the HIBP is considered as a key diagnostic for turbulent transport in the core plasma [17]. In addition, thanks to the fact that the HIBP can measure the k-spectrum of fluctuations (by using multiple entrance slits on the energy analyser), the diagnostic has been used extensively in the research of anomalous transport in tokamak plasmas. Leading experiments have been carried out on the TEXT and TEXT-Upgrade tokamaks with 500 keV and 2 MeV HIBPs, respectively [18,19], and later with a 500 keV HIBP on the JIPPT-IIU tokamak [20,21]. In these studies, a comprehensive comparison of the fluctuation k-ω spectrum and phase velocities obtained by HIBP and other diagnostics, especially electromagnetic wave scattering, was carried out [22]. However, the differences still remain as open questions. In the T-10 tokamak the potential structure in tokamak plasma heated by Electron Cyclotron Resonance waves was studied with a 200 keV HIBP [23].

Since the discovery of the H-mode in the ASDEX tokamak [24], much attention has been paid to the radial electric field in the edge region [25,26]. Efforts to study the H-mode transition using the HIBP have been carried out on TEXT and JIPPT-IIU, but no clear results have been reported. Recently, a 500 keV HIBP was installed on the JFT-2M tokamak, where a fast change of the edge potential associated with the H-mode transition was observed [27]. However, the causal relation between the radial electric field and transport barrier formation has not yet been clarified.

The idea to measure the poloidal magnetic field using the HIBP [28] goes back to the proposal for the measurement of current density profile on the ST tokamak [6], which was not successful at that time. Current profile measurements have been demonstrated in the TEXT tokamak [29], but the accuracy is not yet as good as the MSE (Motional Stark Effect) diagnostic or the Faraday rotation measurement using a FIR (Far Infra-Red) laser. Less demanding than a current profile measurement is the detection of fluctuating magnetic fields associated with MHD modes. In the TEXT tokamak, the radial profile of the magnetic vector

potential of m = 2 rotating magnetic islands was measured [30].

In all of these HIBP set-ups, the beam trajectory was basically two-dimensional. The beam displacement in toroidal direction was compensated by a toroidal beam deflector, in either the primary or the secondary beam line.

Compared to the situation in tokamaks, the radial electric field or space potential structure is more important in stellarators and other non-axisymmetric tori, because in these devices the particle fluxes are intrinsically non-ambipolar. A 160 keV HIBP was applied in the helical device ATF torsatron [31,32]. Since the beam trajectories are fully three-dimensional in helical magnetic configurations, the geometrical arrangement of the beam injector and the energy analyser is not flexible. The energy analyser has to be placed close to the plasma. The magnetic stray-field affected the measurement accuracy in absolute potential measurements. The observation points in the plasma cross-section were limited as well. At CHS a 200 keV HIBP has been developed with the aim to actively control the trajectory. Sweep plates (octapole type) have been installed in the secondary beam line as well as in the primary beam line. The combination of the electric fields in the two deflectors is used to control the injection angle of the secondary beam in the energy analyser [33]. Full radial scanning for the potential profile measurement was achieved with this method [34].

Reviews of the basic principles and the potential of the diagnostic are found in the excellent papers by A.J. Wootton and P.M. Schoch [1], and by T.P. Crowley and RPI team [2]. A review by Y. Hamada treats the turbulence measurements in the JIPPT-IIU tokamak [21]. Those review papers are basically limited to HIBP applications in tokamak research. The reference [2] is in the special issue of the IEEE Transactions on Plasma Science published on the occasion of Prof. Hickok's retirement. This issue includes other review papers from various HIBP groups in the world. Recent progress in HIBP and contributions to physics understanding for toroidal helical plasmas are found in a series of papers by A. Fujisawa and H. Iguchi, et al. [35-38].

In this paper, two examples of HIBP applications in non-axisymmetric tori are presented to emphasise the diagnostic capabilities which have not been discussed in detail in the previous review papers. These are the measurements of the potential structure in the bumpy torus NBT-1M and the heliotron/torsatron CHS.

2. Basic Principles and Hardware

The diagnostic principle of the HIBP is based on the motion of heavy ions in the electromagnetic field (Fig. 1(a)). A singly ionised heavy ion beam is injected into a magnetically confined plasma. Doubly charged secondary ions are produced by ionisation in the plasma. Their trajectory differs from that of the primary ions due to their smaller Larmor radius. A detector located outside the plasma can select a local position in the plasma by selecting a secondary beam trajectory.

The Lagrangian of the beam ions in electromagnetic field in the non-relativistic limit is

$$L = \frac{1}{2} mv^2 - q\phi + q\vec{v} \cdot \vec{A}$$

where q is the ion charge, ϕ is electrostatic potential and A is the magnetic vector potential. The secondary beam carries information on the field quantities, ϕ and A at the ionisation point.

The spatial resolution or the sample volume is basically determined by the primary beam size and the aperture of the detector, which are both typically of the order of mm. It also depends on the magnetic field configuration and the locations of the beam injector and the detector. Trajectory calculation with finite beam size is necessary to optimise the sample volume. In general, the sample volume is elongated along the beam trajectory as shown in Fig. 1(b). The spatial resolution is better in the direction perpendicular to the beam trajectory.

The temporal resolution depends on the signal level of the secondary ions. The secondary beam intensity is given as [2]

$$I_s = \kappa I_p \frac{q_s}{q_p} F_p F_s \sigma_{ion} (T_e) l_{sv} n_e(r)$$

where I_p is the primary beam current, F_p, F_s are the attenuation factor

$$F_j = \exp\left(-\int \sigma_{ion}^j n_e dl\right) \qquad (j = e, i)$$

due to ionisation etc., σ_{ion} is the ionisation cross-section, which is a function of the electron temperature, l_{sv} is the sample volume length along the primary beam trajectory, n_e is the electron density at the ionization point and κ is the amplification factor due to the secondary emission coefficient of the detector plates. The primary beam current is typically 10 to 100 μA when a thermo-ionic alkali-metal ion source is used. The beam energy so far ranges from 10 keV up to 2 MeV. For plasmas with an electron density of 10^{19} m^{-3} and an electron temperature above 100 eV, the secondary beam

current is about 10 to 100 nA, which is large enough to allow a time resolution in the microsecond range.

Figure 2 shows a typical beam injector, consisting of an ion gun, an accelerating tube, a quadrupole lens for beam focusing and shaping, and toroidal and radial beam deflectors. The accelerator tube and the quadrupole lens are not necessary for beams at energy less than tens of keV, because focusing can be obtained with the lens inside the ion gun. Octapole beam defectors can be used instead of a two-stage deflector [34].

The energy analyser used so far for HIBP diagnostics is the Green-Proca type parallel plate electrostatic energy analyser as shown in Fig. 3 [39]. The advantage of this type of analyser is its second-order focusing characteristic. A split plate detector is generally used, which consists of four metal plates for a
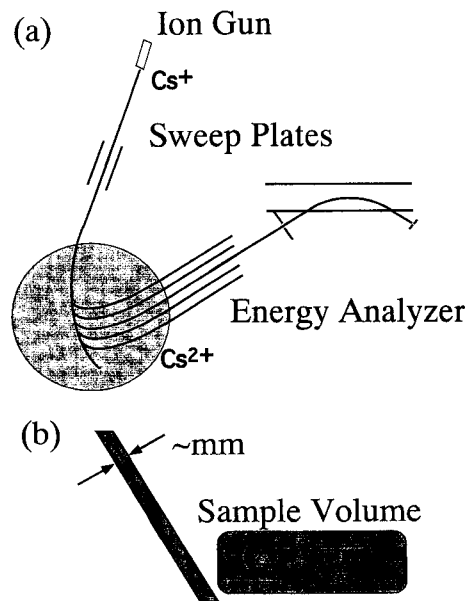

Fig. 1 (a) Basic principles of the heavy ion beam probe. (b) Typical shape of observation volume (sample volume).
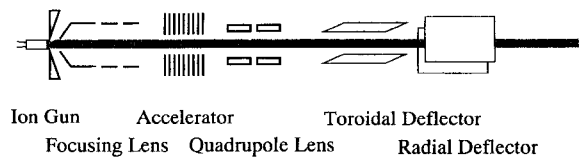

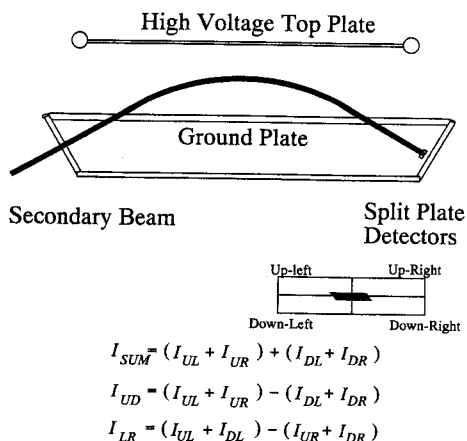Fig. 2 Typical arrangement of beam injector with a thermoionic ion source.

High Voltage Top Plate

Ground Plate

Secondary Beam

Split Plate
Detectors

Up-left | Up-Right

Down-Left | Down-Right

$$I_{SUM} = (I_{UL} + I_{UR}) + (I_{DL} + I_{DR})$$

$$I_{UD} = (I_{UL} + I_{UR}) - (I_{DL} + I_{DR})$$

$$I_{LR} = (I_{UL} + I_{DL}) - (I_{UR} + I_{DR})$$

Fig. 3 Parallel plate energy analyzer with split plate detectors.

single entrance slit. The sum of the beam current on four plates, I_{SUM}, corresponds to the total secondary beam intensity. The beam motion on the detector in the up-down direction, i.e. the up-down difference current (I_{UD}), corresponds to the change of the beam energy. The beam motion in the left-right direction, i.e. the left-right difference current (I_{LR}), corresponds to the toroidal deflection of secondary beam trajectory if the analyser plates are placed horizontally.

A. Electron Density Fluctuations

In low density plasmas, beam attenuation is negligible and the secondary beam intensity I_{SUM} is proportional to the local electron density. The condition for this simple interpretation to hold has been examined, for example, in [40,41]. When attenuation is not negligible, some reconstruction process is required to obtain the local electron density. A HIBP is seldom used for this purpose because there are other diagnostic methods with better accuracy for the electron density measurements. However, the HIBP has been used for density fluctuation measurements because of its good spatial and temporal resolution. The problem arising from the path integral effect has been resolved by utilising a multiple point detection method and taking cross-correlation. Further details on density fluctuation measurements can be found, for example, in [21,42].

B. Electrostatic Potential

From the total energy (kinetic energy + potential energy) conservation before and after the ionisation reaction, the doubly charged secondary ion has an additional energy equal to the local electrostatic

potential at the ionisation point, because the stripped electron removes an amount of energy equal to $-e\phi$. The energy change is resolved at the energy analyser in terms of the difference current I_{UD}. It is noted that the measurement is direct and local. When there are electromagnetic fluctuations in the plasma, the possible change of the beam energy caused by the acceleration due to dA/dt term should be evaluated for all relevant fluctuation models, but it is generally small [43].

C. The Magnetic Vector Potential

The left-right shift of the secondary beam on the split plate detector carries the information on the poloidal magnetic field. This idea has so far only been discussed for axisymmetric tori, for which the canonical angular momentum is conserved. If the symmetry axis is taken in the z direction and the toroidal angle as ζ, it is expressed as

$$P_\varsigma = \frac{\partial L}{\partial \dot\varsigma} = mr^2\dot\varsigma + qrA_\varsigma = \text{const.}$$

Then, the magnetic vector potential at the ionisation point can be expressed as

$$A_{\varsigma i} = \frac{m}{q}\left[\frac{r_d}{r_i}(r_d\dot\varsigma_d) - \frac{r_0}{r_i}(r_0\dot\varsigma_0)\right] + 2\frac{r_d}{r_i}A_{\varsigma d} - \frac{r_0}{r_i}A_{\varsigma 0}$$

where 0, i and d denote the initial, ionisation and detector positions, respectively. All parameters on the right-hand side can in principle be measured, and the local vector potential is obtained. The poloidal magnetic field or plasma current can be calculated if $A_{\varsigma i}$ is measured. In an actual experiment, however, it is difficult to measure the beam velocity in the toroidal direction at the detector. The left-right displacement is measured instead, which is a path integral of the toroidal velocity along the beam trajectory. The fluctuating component of $A_{\varsigma i}$

$$\tilde A_{\varsigma i} = \frac{m}{q}\frac{r_d}{r_i}(r_d\dot\varsigma_d)$$

is more easy to measure because the static part can be dropped.

In real confinement devices there is toroidal field ripple due to the finite number of toroidal coils, so that the system is not truly axisymmetric. In the TEXT tokamak, computer codes were used to derive the local magnetic vector potential [30].

3. Fine Potential Structures
3.1 Static Potential Structures in NBT-1M

A bumpy torus is a closed-line magnetic confinement device containing electrons with energy

from tens of eV to hundreds of keV. The last bumpy torus was shut down more than a decade ago, but bumpy tori have been a treasury of plasma physics. The idea of drift rotational transform due to $E \times B$ poloidal drift as well as grad B and magnetic curvature drifts was tested. The radial electric filed (which is determined by the radial space potential profile) induces poloidal drifts. Closed $E \times B$ drift surfaces are essential for the confinement. Figure 4 shows a grid map of the observation point for the 30 keV HIBP on NBT-1M. By selecting the beam energy and sweep angle, full two-dimensional observation is possible. Figure 5 shows typical contour plots of the space potential for two different operational modes, the C-mode and T-mode. In the collisional regime, the C-mode, the electron temperature was low (10–20 eV) and toroidal drift dominated poloidal drifts. The potential is positive in the upper half of the torus and negative in the lower half of it, which produces a downward electric field resulting in an outward $E \times B$ plasma flow. In the collisionless regime, the T-mode, in which a hot electron ring is formed and the core electron temperature was in the range 50 to 100 eV, poloidally closed potential surfaces are formed. The presence of mirror trapped energetic electrons plays an important role in the formation of the closed $E \times B$ drift surfaces. Figure 6 shows another comparison of potential and density profiles in two different ECH schemes. Poloidal symmetry of the potential profile was improved in this two-frequency ECH operation, which should improve closed contour of the $E \times B$ drift surfaces. Actually a peaked density profile and steeper density gradient were observed. Relation between closed $E \times B$ drift surfaces and particle confinement was also tested using an artificial external error filed. External field was applied artificially by the use of the field correction coils, which were equipped on CHS to cancel intrinsic error field in toroidal average. When the vertical or horizontal field error in the level of $\Delta B/B \sim 2 \times 10^{-4}$ was applied, closed equi-potential contours were destroyed, resulting depression of central electron density and a flattened density profile. Further discussions are found in reference [44].

3.2 Static Potential Structures in CHS

The heliotron/torsatron device CHS is also a non-axisymmetric torus and radial fluxes of electron and ion are not necessarily ambipolar. Effect of space potential profiles or radial electric field on confinement has to be studied. In contrast to the bumpy torus, it has magnetic rotational transform produced by a pair of helical
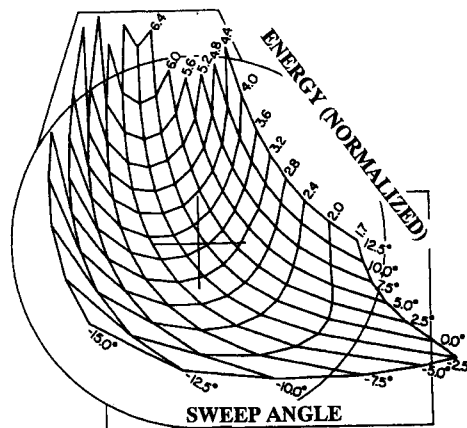

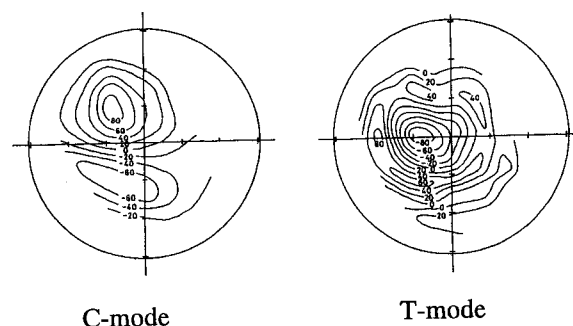Fig. 4 Detection grid on the poloidal cross section in NBT-1M.

C-mode   T-mode

Fig. 5 Two dimensional potential profiles in two different operation regimes in NBT-1M.

18GHzECH   18GHz+8.5GHzECH
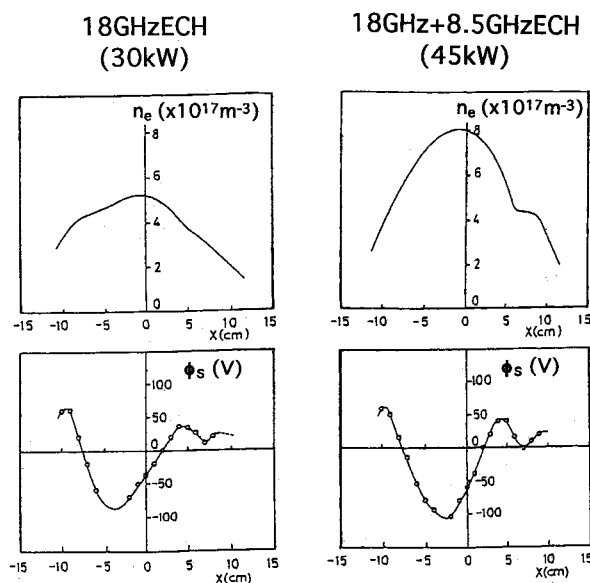(30kW)   (45kW)

Fig. 6 Comparison of density profiles and potential profiles in two different ECH schemes in NBT-1M.

86

windings. Figure 7 (a) shows the schematic diagram of the 200 keV HIBP at CHS. The beam trajectory is completely three-dimensional in this case. Full radial scanning from the top to the bottom of the plasma in
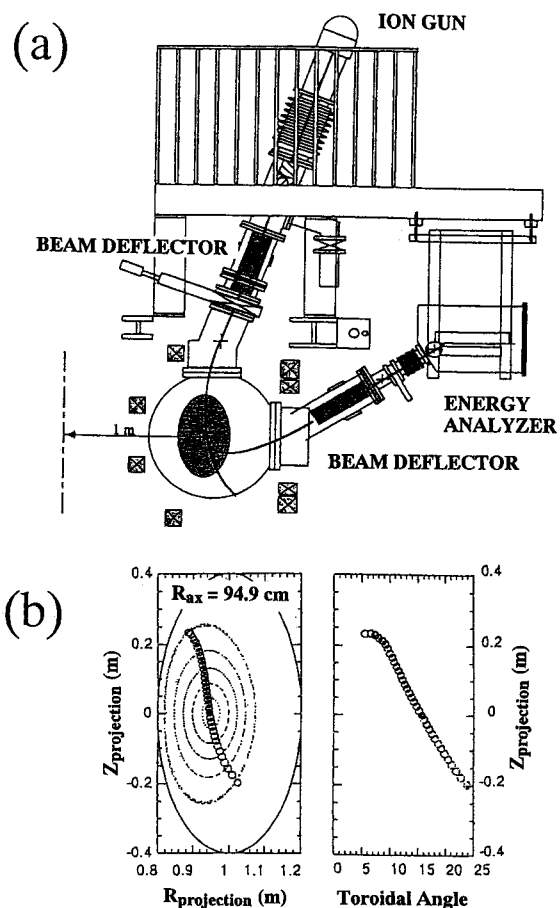

(a)

ION GUN

BEAM DEFLECTOR

ENERGY ANALYZER

BEAM DEFLECTOR

(b)

$R_{ax} = 94.9$ cm

Z projection (m)

R projection (m)   Toroidal Angle

Fig. 7 (a) Schematic of 200 keV HIBP on CHS.
(b) Projection of the observation points on the poloidal cross section for the central scanning chord. Toroidal distribution is also plotted.

300kW ECH
$n_e = 3 \times 10^{18} m^{-3}$
$T_e \gg T_i$

Positive

ECH+NBI
$n_e = 8 \times 10^{18} m^{-3}$
$T_e > T_i$

NBI
$n_e = 8 \times 10^{18} m^{-3}$
$T_e \sim T_i$
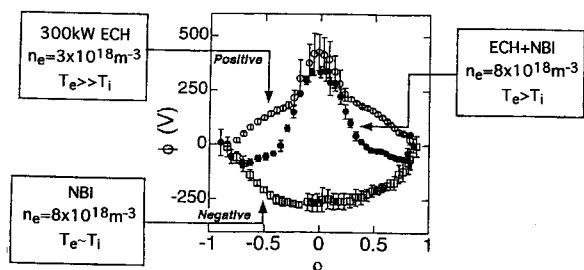
Negative

ϕ (V)

ρ

Fig. 8 Typical potential profiles in different operational regimes in CHS.

poloidal cross section is achieved by the use of the active trajectory control method as shown in the Fig. 7 (b). Various types of potential profile are observed depending on the operational conditions as shown in Fig. 8. The positive ρ corresponds to upper side and the negative ρ, the lower side. A full profile is obtained by sweeping beam in every 2 ms. The electron temperature ranges from 200 eV to 800 eV. The radial electric field is positive in the high T_e ECH plasma and negative in a NBI plasma with comparable T_e and T_i. For the Mexican hat shape, it is considered that electron root and ion root are simultaneously realized in spatially separated regions. The observed potential profiles and the radial electric fields are well explained by neoclassical theory. This does not suggest that electron and ion loss processes be dominated by neoclassical process. In fact transport analysis have shown that anomalous transport dominated in most operation regimes. They are, however, ambipolar and do not effect the flux balance to determine the potential structure. The potential profiles shown in the figure are typical in CHS plasmas, but fine structure changes depending on the heating scheme and plasma collisional parameters.

3.3 Potential Dynamics in CHS

Potential structure in CHS is not always stable, but in some conditions, it exhibits dynamic changes. Figure 9(a) shows temporal variation of the central space potential during a combined ECR+NBI heating. In this case probing beam is fixed to observe the space potential at the plasma center. The time resolution in this operation is of the order of microseconds. Repetitive crush of the central potential is observed approximately in every 2 ms in quasi-steady state. The drop of the central potential reached to 600 eV. Crush occurs in the time scale in the range of several tens microseconds as shown in Fig. 9(b), which clearly suggests that the process is not a diffusive one (~ a few milliseconds). Figure 9(c) is the radial structures of the potential profiles in the two states. It is interpreted as bifurcation phenomena between the two steady state, which is predicted by the neoclassical theory. Because of nonlinear dependence of radial particle fluxes on the radial electric field, multiple steady states solutions can be realized in a non-axisymmetric torus. Detailed physics associated with this bifurcation nature of the potential profiles or radial electric field in a toroidal helical plasmas are described in reference [38] as well as in this conference [47].
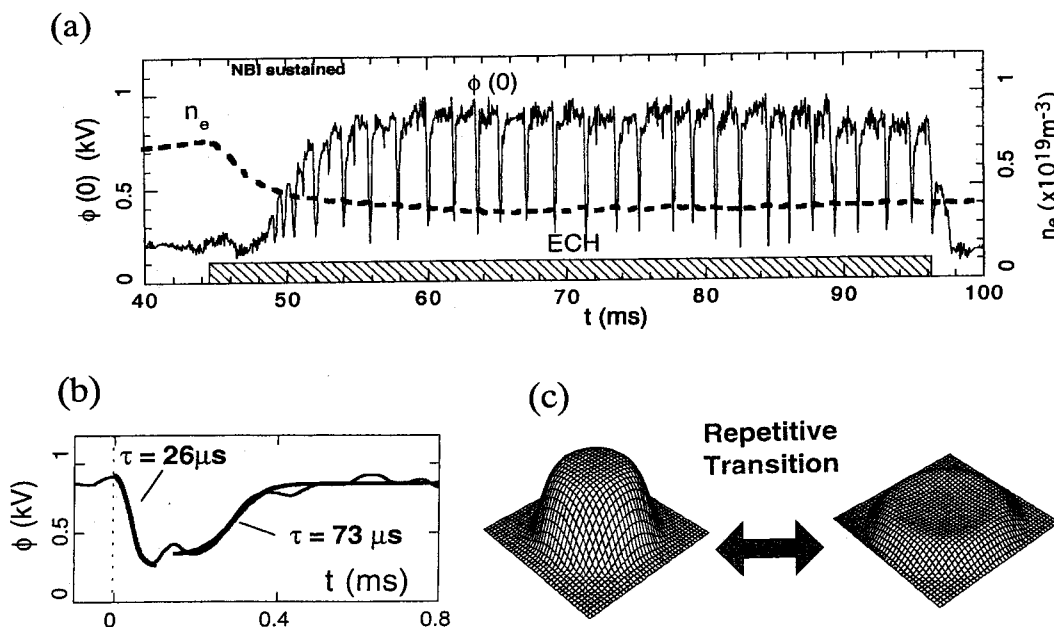
87

(a)

(b)

(c)

Repetitive Transition

Fig. 9 (a) Self-sustained osscillation of space potential observed in a combined ECR+NBI heating.
(b) Fast time scale of the potential crush and recover , suggesting bifurcation phenomenon.
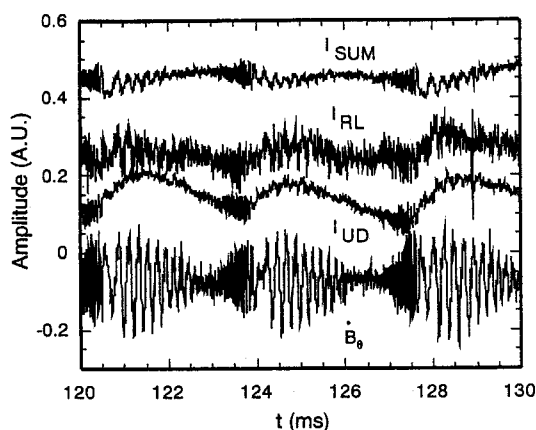(c) Potential profiles before and after the transition.

Fig. 10 HIBP raw signals during the MHD bursts together with a Mirnov coil signal in CHS.
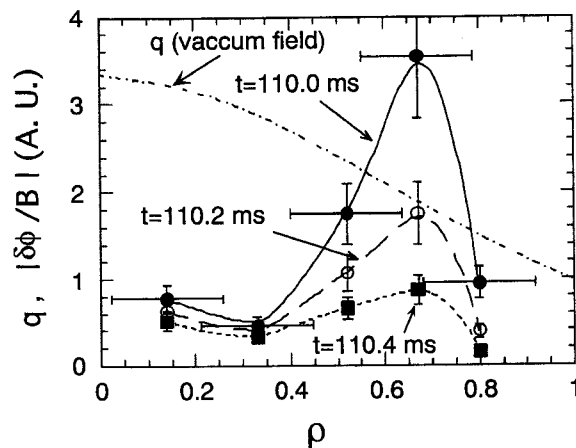

Fig. 11 Radial distribution of space potential oscillation during the growing phase of the MHD burst in CHS.

3.4 Internal Structure of MHD Modes in CHS

Magnetic perturbations associated with MHD instabilities affect the particle trajectory of probing heavy ions. In CHS, the HIBP measurement has been carried out during bursting MHD activity [43]. Figure 10 shows the time behaviour of the raw HIBP signals, I_{SUM}, I_{UD} and I_{LR}, together with the Mirnov coil signal, during the MHD bursts. It is seen that all three signals

are well correlated with the Mirnov coil signals. I_{SUM} includes density fluctuation information but is a path-integrated value. For reconstruction a detailed analysis is required, as mentioned in the previous section. I_{UD} shows the local potential fluctuation. Figure 11 shows radial profiles of the oscillating space potential, which has a peak around the $q = 2$ magnetic surface. The potential oscillation is related with the growth of an $m =$

2 interchange instability. I_{LR} includes toroidal deflection of the beam which comes from the fluctuating vector potential A_ζ. Since the signal is a path-integrated value and magnetic field configuration is not axisymmetric in this case, the radial profile analysis is not straightforward. New algorithms for the reconstruction of the local vector potential are required.

4. Discussion and Summary

Systematic experimental studies on the effect of the radial electric field on confinement have been carried out in the closed-line toroidal system, the bumpy torus NBT-1M. The theoretical framework for the particle confinement in the presence of a radial electric field has been discussed in detail by Kovrizhnikh [45] and Hasting [46]. Multiple solutions of the steady state radial electric field structure were predicted. Steady state solutions are referred to as the electron root and an ion root. The neo-classical theory developed in the bumpy torus research has been extended to the present day discussion for heliotron/torsatron or stellerator confinement physics.

In the toroidal helical system CHS, which has magnetic rotational transform, the potential was observed to be constant on the flux surfaces, in agreement with the general assumption that space potential is a flux function. The poloidal symmetry of the profiles of the potential or the radial electric field in a non-axisymmetric torus with magnetic rotational transform are confirmed in rather wide range of electron or ion collision parameters. However, it is pointed out here that the relation between a small poloidal asymmetry and particle confinement is still an issue to be studied in the present day high temperature confinement devices, like tokamaks and stellarators. The advantage of the HIBP diagnostic is that measurements are local and direct and do not require the assumption that the potential is a flux surface quantity.

Dynamical structural reformation of potential profiles has also been observed in certain operational regimes. The change of the potential profile occurred in the time scale of several tens microseconds, which is much faster than the time scale of diffusion processes. It is interpreted as a bifurcation phenomenon of the radial electric field in toroidal helical plasmas. It has been theoretically predicted, because in such non-axisymmetric tori, multiple solution for the electron and ion flux balance equation can be realised. Different radial electric field corresponds to the different solution. This topic is presented in the separate paper at this conference [47].

Reduced MHD equations have often been used for MHD studies in which the key parameters are the stream function and the poloidal flux function [48]. The stream function is related with the electrostatic potential as

$$\Phi \Leftrightarrow \frac{\phi}{B}$$

and the poloidal flux fluctuation is related with the toroidal component of the magnetic vector potential as

$$\Psi \Leftrightarrow R_0 A_\zeta + \Psi_{vac}$$

Toroidal angular momentum of the probing beam is not conserved in non-axisymmetric toroidal devices. Determination of A_ζ from toroidal displacement of the secondary beam is not direct as in an axisymmetric torus. However, in the heliotron/torsatron configuration, the magnetic structure is mostly determined by the external coils and the vacuum flux function is well determined. The data from CHS show that the oscillating left-right displacement is well correlated with the Mirnov coil signal. The experiment suggests the possibility to measure the toroidal component of vector potential, if the algorithm to reconstruct the vector potential fluctuation component is developed. When the two key parameters of the reduced MHD equations simultaneously with a HIBP, improved understanding of the MHD phenomena in toroidal helical plasmas is expected.

In summary, a heavy ion beam probe is a powerful tool to study the effects of the radial potential structure or the electric field structure on magnetic confinement, especially in non-axisymmetric tori such as a bumpy torus or a stellarator. Short reviews of HIBP development history and basic principles as well as experimental observations are presented emphasising the potential structure measurements in non-axisymmetric tori, which have not been treated in previous HIBP review papers.

Acknowledgement

Ichiguchi. Finally critical reading of the manuscript by refrees is aknowledged.

References

[1] A.J. Wootton and P.M. Schoch, ISPP-9 "Diagnostics for Contemporary Fusion Experiments", p 521 (1991).

[2] T.P. Crowley and RPI team, IEEE Trans. Plasma Sci. 22, 291 (1994).

[3] R.L. Hickok, Rev. Sci, Instrum. 38, 142 (1967).

[4] F.C. Jobes, J.F. Marshall and R.L. Hickok, Phys. Rev. Lett. 22, 1042 (1969).

[5] F.C. Jobes, R.L. Hickok, Nuclear Fusion 10, 195 (1970).

[6] R.L. Hickok and F.C. Jobes, US Air force Office of Scientific Research, No. TR-72-0018 (1972).

[7] J.C. Hosea, F.C. Jobes R.L. Hickok and A.N. Dillis, Phys. Rev. Lett. 30, 839 (1973).

[8] P.L. Colestock, K.A. Connor and R.L. Hickok, Phys. Rev. Lett. 40, 1717 (1978).

[9] F.M. Bieniosek, P.L. Colestock, K.A. Connor, R.L. Hickok and S.P. Kuo, Rev. Sci. Instrum. 51, 206 (1980).

[10] K. Takasugi, H. Iguchi, M. Fujiwara and H. Ikegami, Jpn. J. Appl. Phys. 23, 364 (1984).

[11] E.B. Hooper, Jr., G.A. Hallock and J.H. Foote, Phys. Fluids 26, 314 (1983).

[12] H. Fujita, R. Kumazawa, A.M. Haward, et al., J. Phys. Soc. Jpn. 57, 504 (1988).

[13] K. Ishii, H. Inami, T. Kawabe and S. Miyoshi, Rev. Sci. Instrum. 55, 1924 (1994).

[14] K. Ishii, M. Kotoku, T. Segawa, I. Katanuma, et al., Nuclear Fusion 30, 1051 (1990).

[15] G.A. Hallock, J. Mathew, W.C. Jennings, R.L. Hickok, Phys. Rev. Lett. 56, 1248 (1986).

[16] K. Ida, A. Fujisawa, H. Iguchi, et al., Phys. Plasmas 8, 1 (2001).

[17] R.L. Hickok, P.M. Schoch, T.P. Crowley, J.W. Heard, Proc. 13th Intern. Conf. on Plasma Phys. and Contr. Nucl. Fusion Research, IAEA Vienna, vol. 1, 229 (1991).

[18] P.M. Schoch, J.C. Forster, W.C. Jennings and R.L. Hickok, Rev. Sci. Instrum. 57, 1825 (1986).

[19] R.L. Hickok and P.M. Schoch, Rev. Sci. Instrum. 59, 1685 (1988).

[20] Y. Hamada, et al., Rev. Sci. Instrum. 66, 321 (1995).

[21] Y. Hamada, Fusion Engineering and Design 34-35, 25 (1997).

[22] D.W. Ross, R.V. Bravenec, Ch. P. Ritz, et al., Phys. Fluids B 3, 2251 (1991).

[23] A.V. Melnikov, K.N. Tarasyan, V.A. Vershkov, et al., IEEE Trans. Plasma Sci. 22, 363 (1994).

[24] F. Wagner, G. Becker, et al., Phys. Rev. Lett. 49, 1408 (1982).

[25] S.-I. Itoh, K. Itoh, Phys. Rev, Lett. 60, 2276 (1988).

[26] K. Itoh, S.-I. Itoh, H. Sanuki, A. Fukuyama, IEEE Trans. Plasma Sci. 22, 376 (1994).

[27] T. Ido, K. Kamiya, Y. Miura, Y. Hamada, et al., Plasma Phys. and Control. Fusion 42, A309 (2000).

[28] G. Tonetti and K.A. Connor, Plasma Phys. 22, 361 (1980).

[29] J.G. Schwelberger, PhD Thesis, Rensselaer Polytechnic Institute (1994).

[30] V.J. Simcic, T.P. Crowley, et al., Phys. Fluids B 5, 1576 (1993).

[31] J.J. Zielinski, Rev. Sci. Instrum. 61, 2961 (1990).

[32] K.A. Connor, J.J. Zielinski, J.G. Schwelberger, S.C. Aceto, et al., Rev. Sci. Instrum. 63, 4505 (1992).

[33] A. Fujisawa, H. Iguchi, et al., Rev. Sci. Instrum. 63, 3694 (1992).

[34] A. Fujisawa, H. Iguchi, S. Lee, T.P. Crowley, et al., Rev. Sci. Instrum. 67, 3099 (1996).

[35] A. Fujisawa, H. Iguchi, H. Sanuki, et al., Phys. Rev, Lett. 79, 1054 (1997).

[36] A. Fujisawa, H. Iguchi, H. Sanuki, et al., Phys. Rev, Lett. 81, 2256 (1998).

[37] A. Fujisawa, H. Iguchi, T. Minami, et al., Phys. Rev, Lett. 82, 2669 (1999).

[38] A. Fujisawa, H. Iguchi, T. Minami, et al., Phys. Plasmas 7, 4152 (2000).

[39] T.S. Green and G.A. Proca, Rev. Sci. Instrum. 41, 1409 (1970).

[40] D.W. Ross, et al., Rev. Sci. Instrum. 63, 2232 (1992).

[41] A. Fujisawa, H. Iguchi, et al., Rev. Sci. Instrum. 68, 3393 (1997).

[42] T.P. Crowley, P.M. Schoch, J.W. Heard, et al., Nucl. Fusion 32, 1295 (1992).

[43] S. Lee, H. Iguchi, et al. J. Phys. Soc. Jpn. 67, 3107 (1998).

[44] H. Iguchi, K. Takasugi, et al., IEEE Trans. Plasma Sci. 22, 410 (1994).

[45] L. Kovrizhnykh, Nuclear Fusion 24, 851 (1984).

[46] D.E. Hastings and T. Kamimura, Nuclear Fusion 24, 473 (1984).

[47] A. Fujisawa, Invited talk of this conference.

[48] K. Ichiguchi, Y. Nakamura, M. Kawatani, et al., Nucl. Fusion 29, 2093 (1989).